Materials Chemistry and Physics 116 (2009) 638–644

Contents lists available at ScienceDirect

Materials Chemistry and Physics

journal homepage: www.elsevier.com/locate/matchemphys

Growth and characterization of iron oxide nanocrystalline thin films via low-cost ultrasonic spray pyrolysis

Rajendra N. Goyal[a,*], Davinder Kaur[b], Ashish K. Pandey[a]

[a] Department of Chemistry, Indian Institute of Technology Roorkee, Roorkee 247667, India
[b] Department of Physics & Center of Nanotechnology, Indian Institute of Technology Roorkee, Roorkee 247667, India

ARTICLE INFO

Article history:
Received 31 January 2009
Received in revised form 18 April 2009
Accepted 3 May 2009

Keywords:
Spray pyrolysis
Fe_2O_3 nanopowder
Thin films
Phase transformation

ABSTRACT

The preparation and characterization of iron oxide nanocrystalline thin films by ultrasonic spray pyrolysis technique is reported. Iron oxide films were grown on quartz substrate at different deposition temperatures varying from 400 °C to 700 °C. Both orientation and the size of the crystallites were found to depend on the substrate temperature. The XRD results of nanocrystalline thin films revealed the magnetite to hematite phase transformation with increase in substrate temperature. The morphological characterization of these films by Field emission scanning electron microscopy and Atomic force microscopy showed a grain growth from needle to plate like shape and size distribution in the range of 50–100 nm. The deposited thin films exhibited the estimated direct band gap (E_g) in the range 2–2.2 eV. A comparison of the various properties of thin film and nanopowder of iron oxide are also presented.

1. Introduction

Thin films of iron oxide have attracted considerable attention in last few years due to their interesting magnetic properties. The half-metallic magnetite Fe_3O_4 is highly spin polarized in nature and is desirable for tunneling magneto-resistance based device applications [1]. Materials in nanometer range are found to exhibit new functional properties for a wide range of applications. Magnetic nanoparticles of iron oxide due to its biocompatibility, catalytic activity and low toxicity have dragged significant attention for their applications in various fields of medical care such as drug delivery system, cancer therapy, and magnetic resonance imaging [2–4]. Apart from the biomedical applications, these iron oxide nanoparticles are of technological importance due to their application in many fields including high density magnetic storage devices, ferro-fluids, magnetic refrigeration systems, catalysis and chemical/biological sensors [5,6].

Several type of crystal structures and compositions are found to associated with Iron oxides, like wustite (FeO), which has a rock salt phase, magnetite (Fe_3O_4) and maghemite (γ-Fe_2O_3), having cubic spinel structure [7]. Hematite is isostructural with corundum. The unit cell is hexagonal with $a = 0.5034$ nm and $c = 1.375$ nm. The structure of hematite can be described as consisting of hcp arrays of oxygen ions stacked along the [0 0 1] direction, i.e. planes of anions are parallel to the (0 0 1) plane. Two third of the sites are filled with Fe^{III} ions which are arranged regularly with two filled sites being followed by one vacant site in the (0 0 1) plane thereby forming six-fold rings. The oxygen and Fe arrangement forming Fe–O_3–Fe triplet structure influences the magnetic properties of the oxide. Structural relationships exist between certain planes in the hematite structure and those in other iron oxides, namely magnetite and goethite. There is, for example, a relationship between the (1 1 1) plane of magnetite and (0 0 1) plane of hematite, hence nucleation and growth of the magnetite on the (0 0 1) plane of hematite is sometimes observed. Stoichiometric hematite is a n-type semiconductor and the bandgap is commonly considered to be 2.2 eV. Certain properties of hematite—its ability against dissolution at pH >4 and the fact that a reasonable amount (29%) of visible light has energies greater than the hematite band gap (2.2 eV) have prompted investigation into use of this oxide as an anode for photo assisted electrolysis of water for hydrogen production [8].

Out of these Magnetite (Fe_3O_4) is known for having highest Curie temperature (~860 K). In the cubic inverse spinel structure of Fe_3O_4, iron cations occupy interstices of a face-centered-cubic closed packed array of oxygen ions (lattice parameter ~8.396 Å) [9]. The eight tetrahedral sites of the cube are occupied by Fe^{3+} ions whereas the sixteen octahedral sites are equally shared by Fe^{3+} and Fe^{2+} ions. The rapid hopping of electrons between Fe^{2+} and Fe^{3+} ions in the octahedral sites results in good room temperature conductivity to Fe_3O_4 [10], specifically ρ ~35,000 μΩ cm (ρ: resistivity, polycrystalline film) [11].

A variety of techniques have been used to fabricate iron oxide thin films such as pulsed laser deposition (PLD) [12], sol–gel [13], sputtering [14,15], and molecular beam epitaxy (MBE) [16]. Com-

* Corresponding author. Tel.: +91 1332 285794; fax: +91 1332 273560.
E-mail addresses: rngcyfcy@iitr.ernet.in, rngcyfcy@rediffmail.com (R.N. Goyal).

0254-0584/$ – see front matter © 2009 Elsevier B.V. All rights reserved.
doi:10.1016/j.matchemphys.2009.05.002

pared to other vacuum deposition techniques, spray pyrolysis offers the possibility of preparing small as well as large area coating of iron oxide thin films and nanopowder at low cost for various technological applications. Unlike physical vapour deposition methods, spray pyrolysis does not require high quality target and nor does it require vacuum at any stage, which is a great advantage if the technique is to be scaled up for the industrial applications. Moreover, in spray pyrolysis technique, the deposition rate and the thickness of the films can be easily controlled over a wide range by changing the spray parameters, thus eliminating the major drawbacks of chemical methods such as sol–gel, which produces films of limited thickness [17]. Earlier the successful preparation of nanocrystalline ZnO thin films by the same technique have been reported [18].

In the present study, we have used the simple and low cost ultrasonic spray pyrolysis technique to grow iron oxide nanocrystalline thin films. Further, we have also tried to correlate the structural and optical properties of iron oxide nanocrystalline thin films with nanopowder.

2. Experimental details

Iron oxide thin films were prepared from aqueous solution of Ferric Chloride ($FeCl_3{\cdot}6H_2O$) (purity 99%, Sigma–Aldrich, USA) by dissolving it in distilled water to a concentration of 0.1 M. The substrates were first ultrasonically degreased with acetone, ethanol and deionised water. The designed setup for ultrasonic spray pyrolysis technique is shown in Fig. 1. Ferric Chloride precursor solution was poured in to the vessel from inlet side. The ultrasonic nebulizer (Model NE-U17, Omron Matsusaka Co. Ltd., Japan), which contains 1.67 MHz transducer, atomizes the chemical solution into the stream of fine droplets. The vibration of the transducer converts the precursor solution into the aerosol. The nebulized spray, which goes up in the column, was deposited on a hot substrate, which was further heat treated to get the high quality films. Specially designed digital substrate heater with temperature controller from Excel instruments, Mumbai, India was used to heat the substrate. The rate of deposition was controlled by the carrier gas flow rate, substrate temperature as well as precursor concentration. To make precursor solution, ferric chloride was dissolved in double distilled water. The choice of solution concentration is crucial for the successful deposition of iron oxide thin films. Methanol was added to adjust the concentration of the final solution and to enhance the rate of evaporation. Solutions of various concentrations were tried to optimize the right stoichiometry of the films. It is observed that when spray solution is of high concentration, the cracks start appearing over the films and surface of the films becomes rough. On the other hand, with very dilute spray solution, the films are porous and have voids. Finally, the solution of concentration 0.10 M was found to give good quality films. For the preparation of good quality films, various parameters such as nozzle to substrate distance, deposition rate and flow rate of air (carrier gas), deposition temperature and concentration were optimized to get good quality films. The optimized parameters used are presented in Table 1.

The substrate temperature was calibrated by placing a thermocouple temporarily at the substrate position and simultaneously measuring the temperature of the control thermocouple inside the heater plate. After the spraying procedure, the hotplate was switched off and the samples were subsequently cooled in air. The orientation and crystallinity of the thin films were studied using Bruker AXS C-8 advanced diffractrometer in θ–2θ geometry. The surface topography and microstructure were studied using scanning probe microscope (NT-MDT: NTEGRA Model) and field emission scanning electron microscopy (FE-SEM). Varian Cary-5000 UV–vis–NIR spectrometer was used to study the optical properties of thin films.

Table 1
Optimized spray parameters used for the preparation of Iron oxide thin films.

Spray mode	Ultrasonic nebulizer
Air blast	Atomizer
Ultrasonic frequency (MHz)	1.67
Droplet size (μm)	2.89
Solution flow rate (ml h^{-1})	10
Distance from heater to substrate (cm)	5
Solvent	Distilled water and methanol
Precursor	Ferric chloride hexa hydrate
Concentration (mol l^{-1})	0.1
Deposition temperature (°C)	400, 500, 600, and 700 °C
Substrate	Quartz

To check the conductivity of the prepared thin films for voltammetric purposes, the electrode of the thin films deposited on quartz at different temperatures were made by making a contact of the film with a copper strip and then the whole assembly was wrapped with a good quality scotch tape keeping a hole of 3 mm dia in the tape just above the film to expose that particular area of the film to be in contact with the electrolyte solution. The electrochemical experiments were carried out using computerized BAS (Bioanalytical Systems, West Lafayette, USA) CV-50 W voltammetric analyzer. Electrochemical studies were performed using a conventional three electrode glass cell with a platinum wire as an auxillary electrode and Ag/AgCl electrode as reference (model MF- 2052 RB-5B). The thin film electrode was used as the working electrode. Phosphate buffer of pH 7.2 (μ = 0.1 M) was used for recording voltammograms. All potentials were measured at room temperature with reference to Ag/AgCl electrode.

3. Results and discussion

3.1. Fe_2O_3 nanocrystalline thin films

Fe_2O_3 thin films were deposited using ultrasonic spray pyrolysis on quartz substrate at various deposition temperature in the range 400–700 °C. The chemical solution was atomized into the stream of the fine droplets via ultrasonic nebulizer operated to an atomizing frequency of 1.67 MHz. Chloride precursor solution was poured into the vessel from inlet side. The aerosol was generated from the vibration of the transducer. The nebulized spray, which goes up in the column, was deposited on a hot substrate. The average diameter of the misted droplet can be approximately calculated from an expression given by Lang [19]:

$$D_d = 0.34\left(\frac{8\pi\gamma}{\rho f^2}\right)$$

Where D_d is the droplet diameter, γ is the solution surface tension (72.9×10^{-3} N m^{-1}; surface tension of pure water), ρ is the solution density (1027 kg m^{-3}), and f is the applied ultrasonic frequency (1.7 MHz). The diameter of the misted droplets was calculated using the above parameters and was about 2.89 μm. The mean diameter of the particles (D_p) formed from the misted droplet was theoreti-

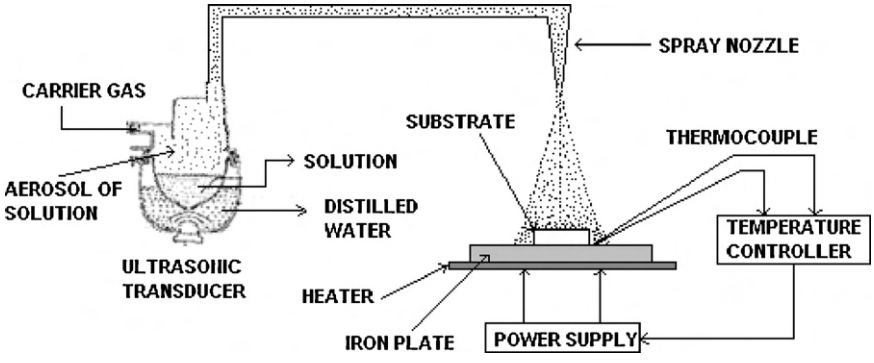

Fig. 1. Schematic diagram of ultrasonic spray pyrolysis setup.

cally calculated using the following equation [20]:

$$D_p = D_d \left(\frac{C_{pr} M_{comp}}{\rho_{comp} M_{pr}} \right)$$

where D_p is the mean diameter of the particles (Fe-oxide) fabricated through pyrolysis reaction, C_{pr} is the precursor concentration ($0.1\ mol\ l^{-1}$), M_{comp} is the molecular mass of the compound, ρ_{comp} is the theoretical density of the compound and M_{pr} is the molecular mass of the precursor. Substituting the D_d value (the diameter of the misted droplet) and the constants into above equation the theoretical mean diameter of Fe-oxide powder was found to be approximately 403 nm.

Fig. 2(A) shows the XRD patterns of iron oxide thin films grown by ultrasonic spray pyrolysis on quartz substrate at various deposition temperatures. The film deposited on quartz at the substrate temperature (T_s) of 400 °C was found to be amorphous whereas the film deposited at T_s = 500 °C was crystalline in nature. The results show that the increase of substrate temperature is in favour to the diffusion of atoms absorbed on the substrate and accelerates the migration of atoms to the energy favorable positions, resulting in the enhancement of the crystallinity [18]. The film deposited at T_s = 500 °C showed the (3 1 1) reflection of magnetite phase whereas the films deposited at T_s = 600 °C were found to be of mixed phase with both the orientations, i.e. (3 1 1) of magnetite phase and (1 0 4) of hematite phase. The only (1 0 4) reflection of pure hematite phase was observed as the substrate temperature was increased to 700 °C. The reason behind this may be due to the fact that at lower substrate temperatures the energy supplied was not sufficient to convert all the Fe atoms to its +3 oxidation state, some Fe atoms get oxidized to its +2 state only and results in $FeO{\cdot}Fe_2O_3$, i.e. magnetite phase. While at higher substrate temperatures, due to sufficient supplied energy, all the Fe atoms get oxidized to its +3 oxidation state which leads to formation of pure hematite phase (Fe_2O_3).

In contrast to the thin films, the room temperature XRD pattern of Fe_2O_3 nanopowder (Fig. 2B) was found to exhibit hematite phase because during synthesis, the temperature of heating zone was kept at 1000 °C in the presence of air as a carrier gas which fully oxidizes the chemical mist of ferric chloride precursor solution. The XRD results indicated that the synthesized Fe_2O_3 powders had the pure hematite structure with lattice parameter a = 1.418 Å and c = 5.363 Å at room temperature. The in-situ high temperature X-ray diffraction of α-Fe_2O_3 nanopowder at increasing temperature from room temperature to 1100 °C showed a clear phase change due to vacuum annealing of the powder (Fig. 2C). The hematite phase changes to magnetite phase above 300 °C which could be due to the fact that with increase in temperature, the oxygen partial pressure decreases, which creates reducing atmosphere and results in the

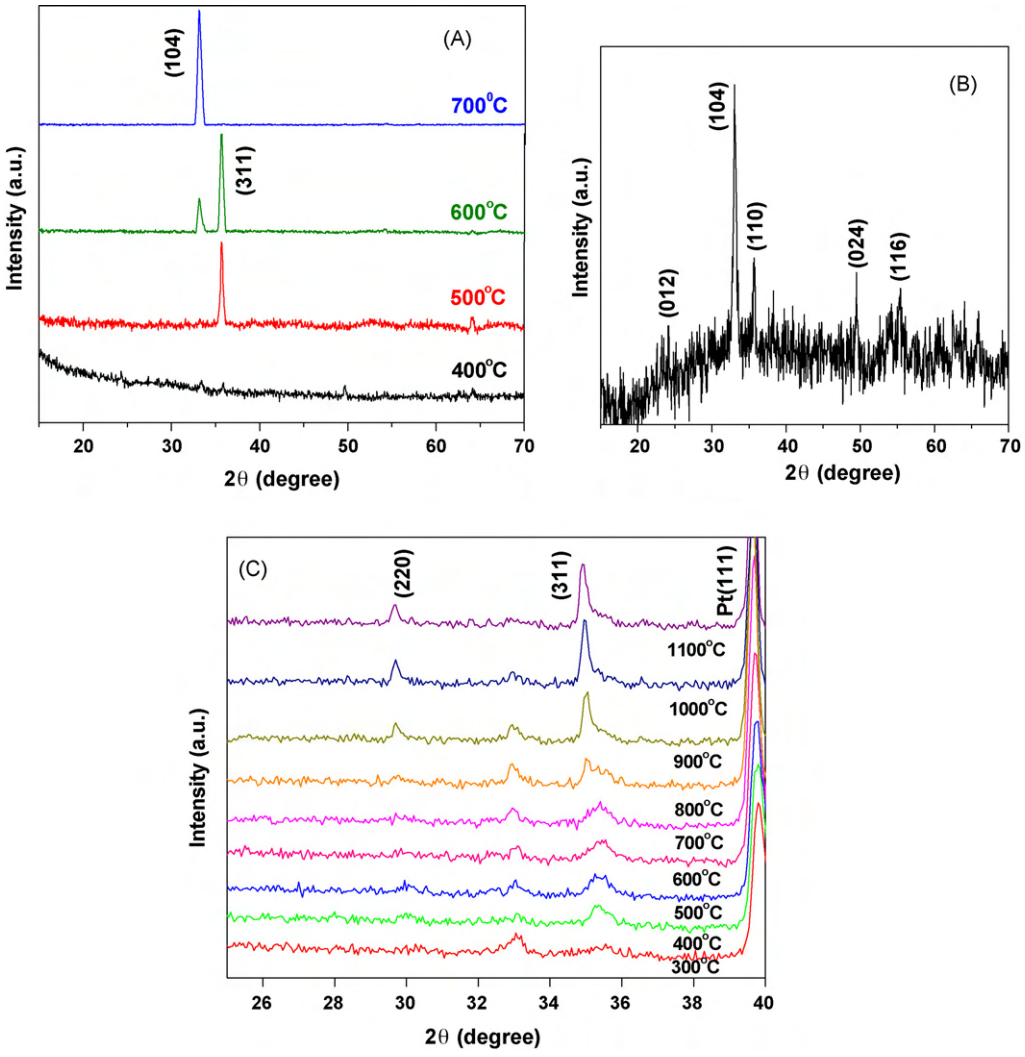

Fig. 2. (A) Room temperature XRD spectra of the Fe_2O_3 nano thin films at various depositions temperatures, (B) room temperature XRD spectra of the Fe_2O_3 nanopowder and (C) high temperature XRD spectra at various temperatures.

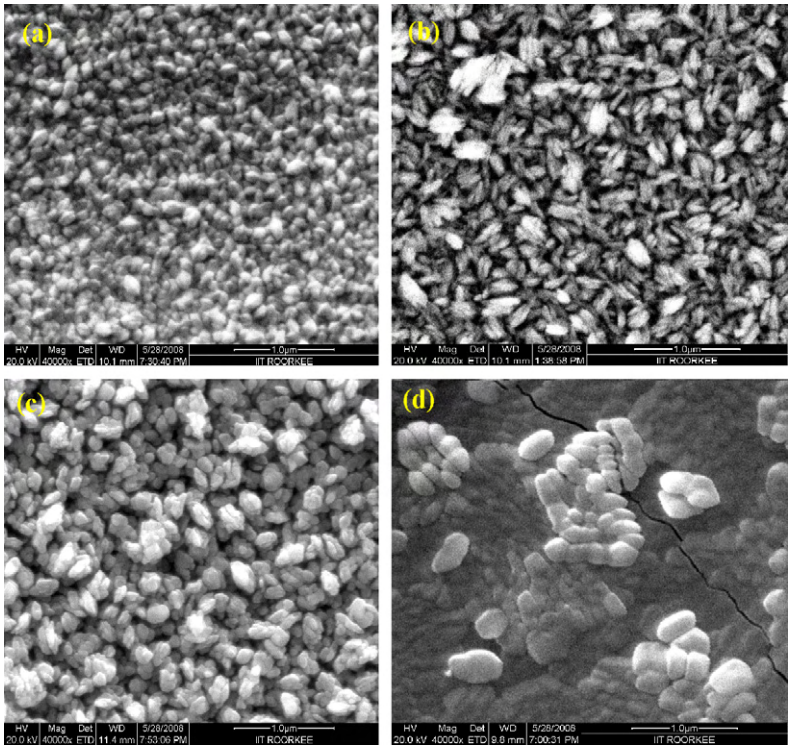

Fig. 3. FE-SEM image of iron oxide nano thin films at (A) 400 °C (B) 500 °C (C) 600 °C and (D) 700 °C.

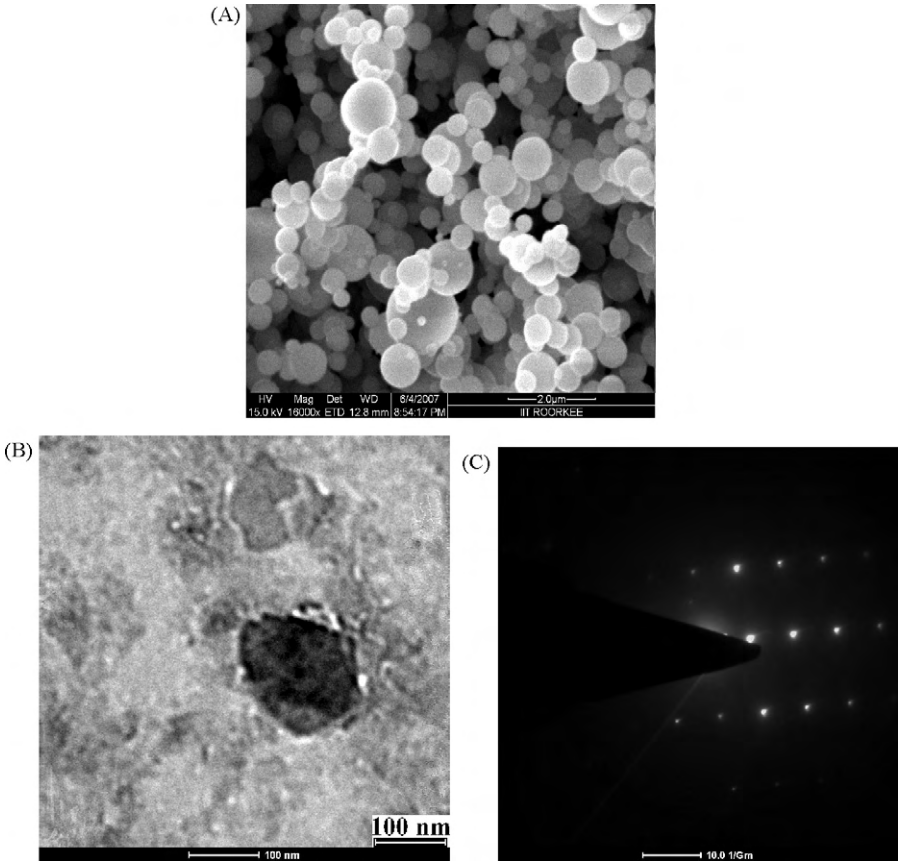

Fig. 4. (A) FE-SEM image of Fe_2O_3 nanopowder, (B) TEM image and (C) corresponding diffraction pattern of prepared nanopowder.

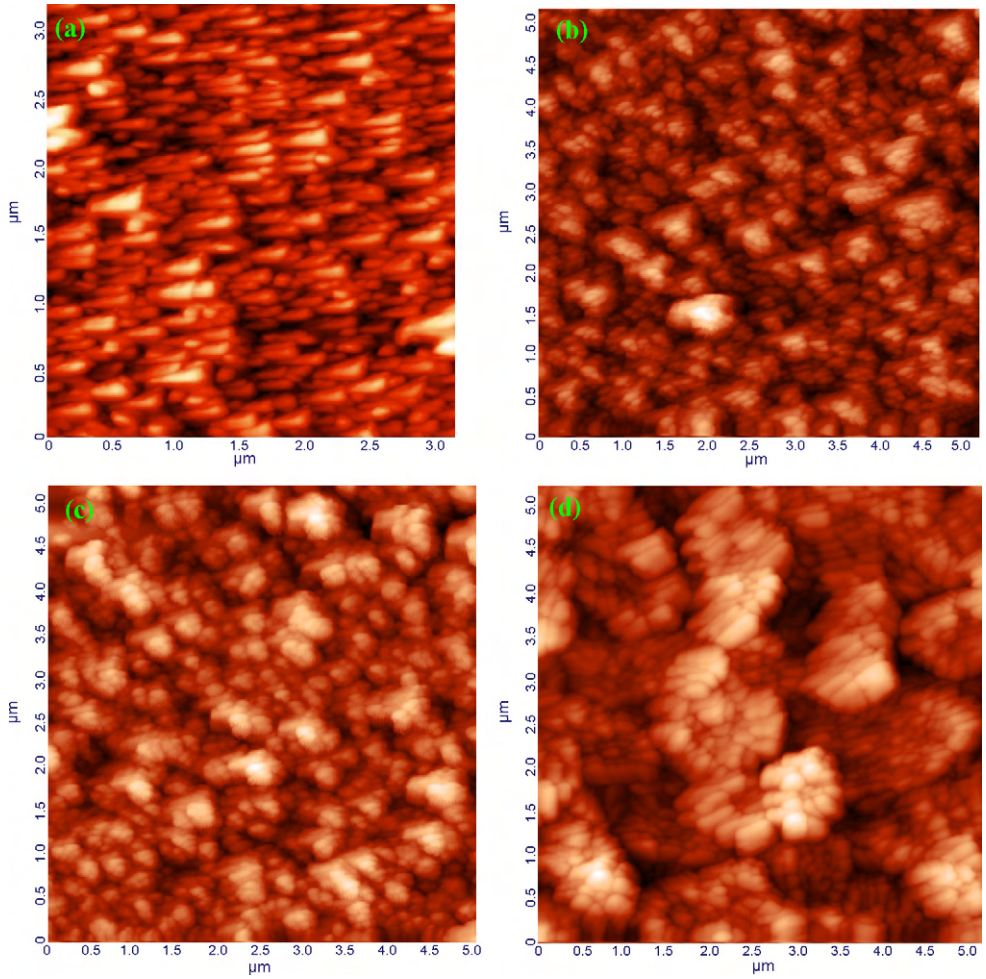

Fig. 5. AFM image of iron oxide nano thin films at (A) 400 °C (B) 500 °C (C) 600 °C and (D) 700 °C.

reduction of Fe^{3+} to Fe^{2+} and hence the magnetite phase appeared with increasing temperature [21,22].

Fig. 3(A–D) shows the FESEM images of iron oxide thin film grown on quartz at different deposition temperatures. The micrograph of the film deposit at substrate temperature of 500 °C shows needle type grain growth while shape of the grains were found to be changed from granular to plate like with change in substrate temperature from 600 °C to 700 °C. Also, it is clearly visible that the particle size increases with increase in deposition temperature. The particle size shown by FESEM was much higher as compared with that calculated from the XRD results. This was because of the fact that the XRD gave the average mean crystallite size while FESEM showed agglomeration of the particles. The XRD and FESEM data can be reconciled by the fact that smaller primary particles have a large surface free energy and would, therefore, tend to agglomerate faster and grow into larger grains.

The morphology of Fe_2O_3 nanopowder as revealed by FE-SEM (Fig. 4A) showed spherical nanoparticles of size approx. 50–100 nm. The morphology and structure of powder was also investigated by TEM. Bright field TEM images and the corresponding diffraction pattern for Fe_2O_3 nanopowder are shown in Fig. 4(B and C). It can be seen that the powder consists of several nanometer spherical particles, which is consistent with the XRD and FE-SEM results. However, part of small particles aggregated into secondary particles because of their extremely small sizes and high surface energies. Therefore it is difficult to precisely determine the size and size distribution of the nanoparticles by simply viewing the TEM image. From the electron diffraction (ED) pattern of the sample, the hexagonal structure of hematite is identified and the reflection planes (1 0 4) and (1 1 0) are clearly seen.

The surface morphology of the thin films was also studied using atomic force microscope (NT-MDT: NTEGRA Model) over 3 mm × 3 mm area in semi-contact mode. Fig. 5(A–D) shows the AFM images of the films deposited on the quartz substrate that supported the FESEM results. The AFM images also support the change in microstructure with change in temperature along with agglomeration of the particles. The average surface roughness was also calculated using AFM micrographs and found to be 16.52 nm, 23.22 nm, 31.8 nm and 36.27 nm for the film deposited at substrate temperature of 400 °C, 500 °C, 600 °C and 700 °C, respectively.

Fig. 6 (A and B) shows the energy band gap and the optical transmittance spectra of Fe_2O_3 thin films, respectively. In order to calculate the direct band gap, we used the Tauc's relationship was used as follows:

$$\alpha h\nu = A(h\nu - E_g)^n$$

where α is the absorption coefficient, A is a constant, h is Planck's constant, ν is the photon frequency, E_g is the optical band gap energy, and n is the 1/2 and 2 for the transition being direct and indirect respectively [23,24]. An extrapolation of the linear region of a plot of $(\alpha h\nu)^2$ on the y-axis versus photon energy $(h\nu)$ on the x-axis gives the value of the optical band gap E_g. Since $E_g = h\nu$ when $(\alpha h\nu)^2 = 0$.The film deposited at substrate temperature of 400 °C exhibited higher band gap as compared to the film deposited at 500 °C, which could be due the enhancement in crystallinity with

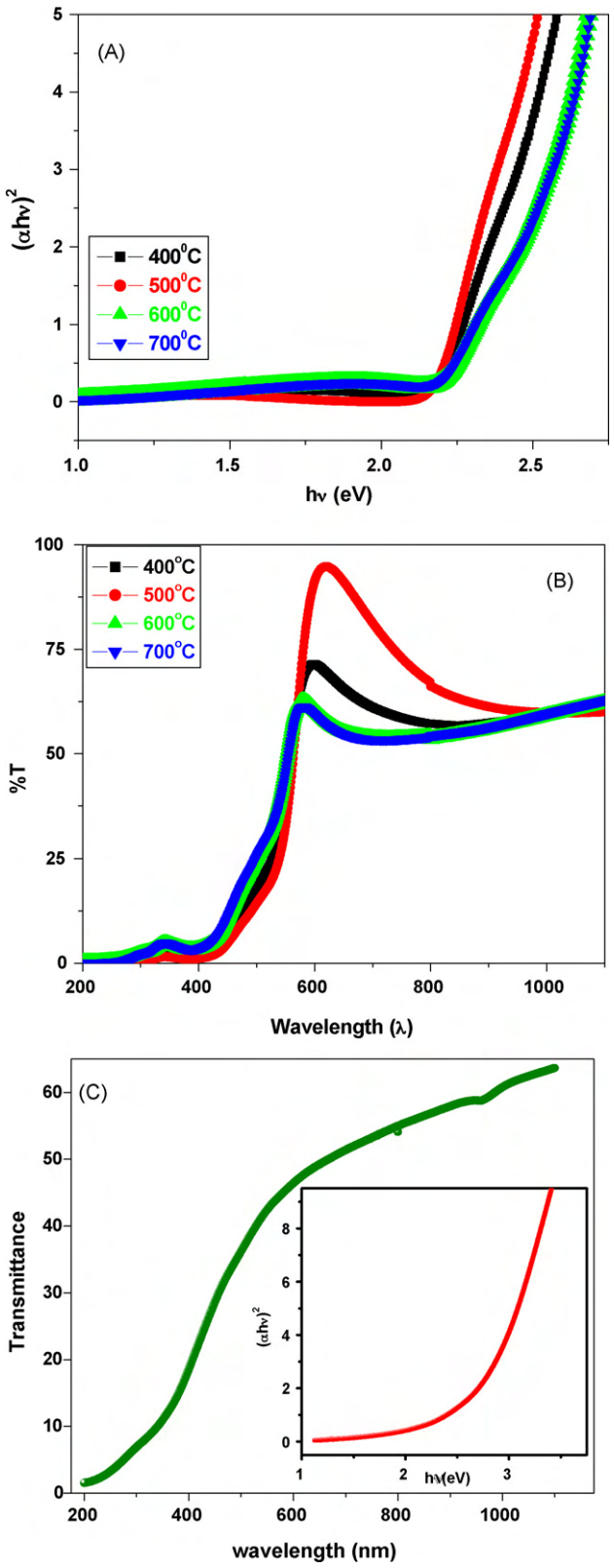

Fig. 6. (A) Energy band gap, (B) optical transmittance spectra of thin films at various deposition temperatures and (C) optical transmittance spectra (Energy band gap in inset) of nanopowder.

increase in substrate temperature that leads to lesser defects and better crystal structure. The films deposited at 600 °C and 700 °C show slightly higher band gap than that of the film deposited at 500 °C. The reason could be attributed to the presence of hematite phase in case of the films deposited at 600 °C and 700 °C, which exhibit higher band gap as compared to magnetite phase. The calculated band gap for the Fe_2O_3 nanopowder was found to be near 2.5 eV as reported earlier [17].

Fig. 6(C) shows the transmittance spectra of the thin films in the wavelength range 200–1100 nm. Transmittance of the film deposited at 500 °C was found to be higher as compared to the film deposited at 600 °C and 700 °C. The transmittance is expected to depend on several factors, such as oxygen deficiency, surface roughness, and impurity centers. The average value of transmittance in the transmittance spectra of α-Fe_2O_3 nanopowder was also found to be about 55% in the visible range of electromagnetic radiation. The lower value of transmittance could be due to light scattering from rough surface and defect states.

3.2. Low conductivity of thin films

To monitor the conductivity voltammetric response of thin film electrode was recorded for dopamine, a well known compound exists in human system,. It was found that the electrodes made from thin films prepared at 400 °C and 500 °C exhibited low current (of the order of nanoampere) even for millimole solution of dopamine and, therefore suggested that the conductivity of these films is low. Such a low current is not useful for determination purposes. Also the peak was not clear for electrodes prepared from thin films. The thin films prepared at 600 °C and 700 °C had almost negligible current with no contact at many points. Thus, the value of current was found to decrease with increase in substrate temperature at which film was deposited. One of the reasons for such a behaviour may be due to the presence of magnetite phase at low deposition temperature, which conducts the current due to electron hopping and hence more conducting as compared to hematite phase which is formed at higher temperature.

4. Conclusion

In summary a comparative study of structural, optical and electrochemical properties of Fe_2O_3 thin films and nanopowder has been presented. In case of Fe_2O_3 thin films, magnetite to hematite phase transformation was observed with increase in deposition temperature from 500 °C to 700 °C while in-situ high temperature XRD results of nanopowder revealed the hematite to magnetite phase transformation. AFM and FESEM micrographs showed the needle type grains in case of the film deposited at 500 °C while granular to plate like structure was observed with further increase in temperature from 600 °C to 700 °C. The band gap in case of the nanopowder was found to be higher as compared to the thin films. The thin films deposited on quartz substrate at different temperatures had low conductivity and thus are not suitable for electrochemical sensing.

Acknowledgement

One of the authors (Ashish K. Pandey) is thankful to the University Grants Commission, India for awarding Junior Research Fellowship.

References

[1] J. Tang, K.Y. Wang, W. Zhou, J. Appl. Phys. 89 (2001) 11.
[2] Xu Jing, Y. Haibin, Fu Wuyou, Du Kai, Yongming Sui, Jiuju Chen, Yi Zeng, Minghui Li, Guangtian Zou, J. Mag. Mag. Mat. 309 (2007) 307.

[3] B. Fang, G. Wang, M. Li, X. Kan, Electroanalysis 17 (2005) 744.
[4] A.K. Gupta, M. Gupta, Biomaterials 26 (2005) 3995.
[5] V. Sreeja, P.A. Joy, Mater. Res. Bull. 42 (2007) 1570.
[6] J. Du, H. Liu, J. Magn. Magn. Mater. 302 (2006) 263.
[7] T. Tepper, C.A. Ross, J. Appl. Phys. 91 (2002) 7.
[8] S.S. Kulkarni, C.D. Lokhande, Mater. Chem. Phys. 82 (2003) 151.
[9] N. Tsuda, K. Nasu, A. Fujimori, K. Shiratori, Elec. Cond. Oxid. (Shokabo, Japan) (1993) 307.
[10] E.J.W. Verwey, Nature (London) 144 (1939) 327.
[11] J.M.D. Coey, A.E. Berkowitz, L.I. Balcells, F.F. Putris, F.T. Parker, Appl. Phys. Lett. 72 (1998) 734.
[12] M.K. Krause, P. Esquinazi, M. Ziese, R. Hohne, A. Pan, A. Galkin, E. Zeldov, J. Magn. Magn. Mater. 245 (2002) 1097.
[13] N.J. Tang, W. Zhong, H.Y. Jiang, X.L. Wu, W. Liu, Y.W. Du, J. Magn. Magn. Mater. 282 (2004) 92.
[14] S. Ohta, A. Tterada, Thin Solid films 143 (1986) 73.
[15] G. Zhang, C. Fan, L. Pan, F. Wang, P. Wu, H. Giu, Y. Gub, Y. Zhang, J. Magn. Magn. Mater. 293 (2005) 737.
[16] W. Eerenstein, L. Kalev, L. Niesen, T.T.M. Palstra, T. Hibma, J. Magn. Magn. Mater. 258–259 (2003) 73.
[17] R.N. Goyal, A.K. Pandey, D. Kaur, A. Kumar, J. Nanosci. Nanotechnol. 9 (2009) 4692.
[18] P. Singh, A. Kumar, Deepak, D. Kaur, J. Crys. Growth 306 (2007) 303.
[19] R.J. Lang, J Acoust. Soc. Am. 43 (1962) 6.
[20] J.M. Nedeljkovie, Z.V. Saponjic, Z. Rakocevic, V. Jakanovic, D.P. Uskokovic, Nanostruct. Mater. 9 (1997) 125.
[21] I.A. Serbinov, G.A. Niklasson, C.G. Granqvist, J. Mater. Sci. 23 (1988) 3876.
[22] A. Petras, K. Preisinger, Mereiter, Mater. Sci. Forum 278 (1998) 396.
[23] L. Dghoughi, B. Elidrissi, C. Bernede, M. Addou, M.A. Lamrani, M. Regragui, H. Erguig, Appl. Surf. Sci. 253 (2006) 1823.
[24] A.A. Akl, Appl. Surf. Sci. 233 (2004) 307.